Int J Fract (2010) 166:225–237
DOI 10.1007/s10704-010-9534-1

ORIGINAL PAPER

Growth of slip surfaces and line inclusions along shear bands in a softening material

F. Dal Corso · D. Bigoni

Received: 22 December 2009 / Accepted: 26 July 2010 / Published online: 11 August 2010

Abstract A perturbative approach applied to pre-stressed elastic solids exhibiting strain softening (of the true-stress/true-strain response) provides an explanation to the common observation that shear bands formed within ductile and quasi-brittle materials tend to grow rectilinearly under Mode II and that slip surfaces tend to nucleate and grow inside them. The effects of an 'obstacle' (a rigid line inclusion) within a shear band are also analyzed and quantified in terms of inhibition of shear band growth.

Keywords Crack · Propagation · Rigid line inclusion · Quasi-brittle material · Large strain

1 Introduction

Common experimental observations in ductile and quasi-brittle materials show that: (i.) shear band formation is a preferential precursor of failure, (ii.) such bands grow rectilinearly under Mode II loading (while cracks tend to deviate from rectilinearity under this condition), (iii.) slip surfaces nucleate and grow within shear bands, leading to 'ultimate' failure. An example of this situation is reported in Fig. 1, where fractures (so-called 'head checks') induced by rolling contact in a steel rail shown formed at approximately 15°–25° with respect to the railway surface. These head checks have developed along shear bands[1] and unless removed from the rail's surface, they continue to grow rectilinearly (with a final change in direction due to an eventual stress redistribution).

The above-mentioned features of shear band propagation and fracture nucleation and growth have remained practically unexplored until the work by Bigoni and Dal Corso (2008), who developed a perturbative approach in which a finite-length slip surface perturbs the state of a ductile infinite material uniformly prestressed near the elliptic boundary. A similar approach has also been developed for a rigid line inclusion (so-called 'stiffener') as perturbing agent (Dal Corso et al. 2008; Bigoni et al. 2008; Dal Corso and Bigoni 2009) showing that shear bands nucleate from the tips of such inclusion. In all these works, ductile materials have been modelled through the J_2–deformation theory of plasticity (Neale 1981).

The J_2–deformation theory of plasticity is a material model tailored to reproduce the loading branch of hardening metals at large strain, typically steel, so that the characteristic softening behaviour representative

F. Dal Corso · D. Bigoni (✉)
Department of Mechanical and Structural Engineering, University of Trento, via Mesiano 77, 38050 Trento, Italy
e-mail: bigoni@ing.unitn.it
URL: http://www.ing.unitn.it/∼bigoni/

F. Dal Corso
e-mail: francesco.dalcorso@ing.unitn.it

[1] Results of calculations performed by Prof. F.D. Fischer (University of Leoben) confirm that the inclination of shear bands is correctly predicted by J_2–flow theory of plasticity.

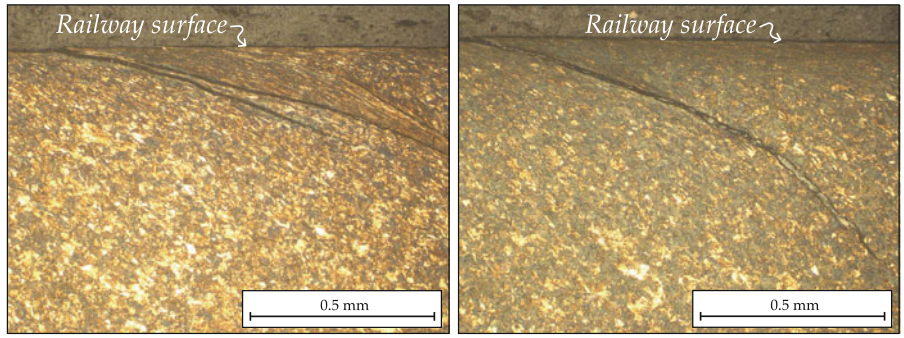

Fig. 1 Slip surfaces, so-called 'head checks', formed along shear bands induced in a heavily deformed, sheared surface of a typical head hardened rail steel (R350HT) due to rolling contact. Courtesy of voestalpine Schienen GmbH

of quasi-brittle materials cannot be properly investigated. To this purpose, Gei et al. (2004) have proposed an incompressible elastic model ('GBG material' in the following) defined for large strain, based on a nonconvex strain energy (written in terms of the logarithmic, also called 'true', strain) and capable of reproducing strain softening in the true-stress/true-strain response. A similar idea (but based on different considerations) has also independently been pursued by Trapper and Volokh (2008) and Volokh (2007) to introduce strain softening in hyperelastic materials. Both models, tested on different boundary value problems, have revealed features about the failure of quasi-brittle materials, so that it may become of interest now to analyze the sensitivity of slip surface and stiffener growth to the state of the material, represented by prestress and anisotropy parameters. Therefore, the aim of this article is to investigate shear band and slip surface growth in softening materials modeled by the GBG elastic model under plane strain condition. Incremental closed-form solutions are presented for a finite-length slip surface and also for a rigid line inclusion embedded in a uniformly prestressed material perturbed by a uniform incremental loading at infinity. The former problem is representative of a pre-existing shear band or a fracture previously nucleated along a shear band, while the latter provides information about the effects of an obstacle to shear band growth. Furthermore, the analysis of incremental energy release rate associated to the inclusion growth allows us to conclude that shear band growth or propagation of a slip surface along a shear band is strongly promoted, while growth of a rigid line inclusion is inhibited. These results therefore complement, confirm and extend to quasi-brittle materials previous investigations by the authors focussed on ductile metallic materials.

2 GBG and J_2–deformation theory of plasticity materials

In general, an elastic incompressible material can be introduced in terms of a strain energy $\widehat{W}(\lambda_1, \lambda_2, \lambda_3)$, function of the principal stretches λ_i corresponding to the Eulerian principal axes $\mathbf{v}_i$ $(i = 1, 2, 3)$, defined in a such way that the principal Cauchy stress tensor $\mathbf{T}$ is given by Ogden (1984)

$$\mathbf{T} = -\pi \mathbf{I} + \lambda_1 \frac{\partial \widehat{W}}{\partial \lambda_1} \mathbf{v}_1 \otimes \mathbf{v}_1 + \lambda_2 \frac{\partial \widehat{W}}{\partial \lambda_2} \mathbf{v}_2 \otimes \mathbf{v}_2 + \lambda_3 \frac{\partial \widehat{W}}{\partial \lambda_3} \mathbf{v}_3 \otimes \mathbf{v}_3, \tag{1}$$

where π is the Lagrangean multiplier related to incompressibility, imposing the following constraint on the stretches

$$\lambda_1 \lambda_2 \lambda_3 = 1. \tag{2}$$

In terms of the principal components of the logarithmic strain ϵ_i,

$$\epsilon_i = \log \lambda_i, \quad i = 1, 2, 3, \tag{3}$$

the strain energy function can be redefined as $W(\epsilon_1, \epsilon_2, \epsilon_3) = \widehat{W}(\lambda_1, \lambda_2, \lambda_3)$ to yield

$$\mathbf{T} = -\pi \mathbf{I} + \frac{\partial W}{\partial \epsilon_1} \mathbf{v}_1 \otimes \mathbf{v}_1 + \frac{\partial W}{\partial \epsilon_2} \mathbf{v}_2 \otimes \mathbf{v}_2 + \frac{\partial W}{\partial \epsilon_3} \mathbf{v}_3 \otimes \mathbf{v}_3, \tag{4}$$

and the incompressibility constraint (2) becomes

$$\epsilon_1 + \epsilon_2 + \epsilon_3 = 0. \tag{5}$$

The simplest modeling of isotropic incompressible materials involves only one strain invariant, namely, the effective logarithmic strain ϵ_e,

$$\epsilon_e = \sqrt{\frac{2}{3}\left(\epsilon_1^2 + \epsilon_2^2 + \epsilon_3^2\right)}, \tag{6}$$

so that different material behaviours are described by introducing different functional dependencies of the strain energy W on ϵ_e.

The GBG elastic incompressible material introduced by Gei et al. (2004) and the J_2–deformation theory of plasticity material Neale (1981) correspond to two different choices of the strain energy function $W(\epsilon_e)$:

- the GBG material is defined by

$$W^{\mathrm{GBG}}(\epsilon_e) = K c\,\epsilon_0 \left[\frac{1}{1+c}\exp\left(-\frac{\epsilon_e}{\epsilon_0}\right) - 1\right] \times \exp\left(-\frac{\epsilon_e}{c\,\epsilon_0}\right), \tag{7}$$

  where K is a positive *stiffness* parameter, while c and ϵ_0 are dimensionless positive parameters;
- the J_2–deformation theory of plasticity material is defined by

$$W^{J_2}(\epsilon_e) = \frac{K}{N+1}\epsilon_e^{N+1}, \tag{8}$$

  where K is a positive *stiffness* parameter and $N \in (0, 1]$ is a *strain hardening* exponent.[2]

Employing Eq. (4) relating stress to strain energy, the principal components of the Cauchy stress T_i can be obtained:

- for the J_2–deformation theory of plasticity material as

$$T_i = -\pi + \frac{2K}{3}\epsilon_e^{N-1}\epsilon_i, \quad i = 1, 2, 3; \tag{9}$$

- for the GBG material as

$$T_i = -\pi + \frac{2}{3}K\frac{\epsilon_i}{\epsilon_e}\left[1 - \exp\left(-\frac{\epsilon_e}{\epsilon_0}\right)\right] \times \exp\left(-\frac{\epsilon_e}{c\,\epsilon_0}\right), \quad i = 1, 2, 3. \tag{10}$$

Note that under plane-strain condition, the in-plane mean stress p,

$$p = \frac{T_1 + T_2}{2}, \tag{11}$$

assumes the same value of the three-dimensional mean stress $(T_1 + T_2 + T_3)/3$, for the J_2–deformation theory material and for the GBG material.[3]

[2] Note that the stiffness parameters K introduced for the J_2–deformation theory of plasticity and for the GBG materials need not to be the same.

[3] This property does not hold in general. In fact, using the generic relation describing an initially isotropic incompressible material

$$T_i = -q + \beta_0\lambda_i^2 + \beta_1\lambda_i^{-2}, \quad i = 1, 2, 3, \tag{12}$$

The principal difference between the J_2–deformation theory material and the GBG model lies in the convexity of the strain energy $W(\epsilon_1, \epsilon_2, \epsilon_3)$. In particular, its Hessian can be written as a function of the derivatives of $W(\epsilon_e)$,

$$\frac{\partial^2 W}{\partial\epsilon_i\partial\epsilon_j} = \frac{2}{3\,\epsilon_e}\frac{dW}{d\epsilon_e}\delta_{ij} + \frac{4}{9\,\epsilon_e^3}\left(\epsilon_e\frac{d^2W}{d\epsilon_e^2} - \frac{dW}{d\epsilon_e}\right)\epsilon_i\epsilon_j, \quad i, j = 1, 2, 3, \tag{15}$$

which has the following eigenvalues (for a generic three-dimensional deformation)

$$\left\{\frac{2}{3\,\epsilon_e}\frac{dW}{d\epsilon_e}, \quad \frac{2}{3\,\epsilon_e}\frac{dW}{d\epsilon_e}, \quad \frac{2}{3}\frac{d^2W}{d\epsilon_e^2}\right\}. \tag{16}$$

Therefore, strict convexity corresponds to strict positiveness of the first and second derivative of $W(\epsilon_e)$ and, consequently,

- the strain energy $W^{J_2}(\epsilon_1, \epsilon_2, \epsilon_3)$, Eq. (8), results to be a strictly convex function for every deformation state;
- the strain energy $W^{\mathrm{GBG}}(\epsilon_1, \epsilon_2, \epsilon_3)$, Eq. (7), *is a nonconvex function*. In particular, convexity is lost for the GBG material for deformation states satisfying

$$\epsilon_e > \epsilon_0 \log(1 + c). \tag{17}$$

In a large strain elasticity framework, the adjectives 'convex' and 'nonconvex' have to be related to a precise

Footnote 3 continued
where q is a Lagrange multiplier related to the incompressibility constraint and β_0 and β_1 are generic stiffness function of the stretches λ_i, when a x_1–x_2 plane-strain state is considered $(\lambda_2 = 1/\lambda_1, \lambda_3 = 0)$, the mean stresses result to be given by

$$\frac{T_1 + T_2 + T_3}{3} = -q + \frac{(\beta_0 + \beta_1)\left(1 + \lambda_1^2 + \lambda_1^4\right)}{3\lambda_1^2}, \qquad p = -q + \frac{(\beta_0 + \beta_1)\left(1 + \lambda_1^4\right)}{2\lambda_1^2}. \tag{13}$$

Therefore, only for particular constitutive models (for which $\beta_0 = -\beta_1$, as in the cases of the J_2–deformation theory and GBG materials) the two mean stresses coincide under the plane strain condition. Under small strain (i.e. neglecting terms higher than first-order), the mean stresses take always the same value independently of the constitutive parameters, as can be easily verified through a Taylor series expansion

$$\frac{T_1 + T_2}{2} \sim \frac{T_1 + T_2 + T_3}{3} \sim [-q + \beta_0 + \beta_1]_{\lambda_1=1} + \left[\frac{d\,\beta_0}{d\,\lambda_1} + \frac{d\,\beta_1}{d\,\lambda_1}\right]_{\lambda_1=1}(\lambda_1 - 1). \tag{14}$$

form of strain energy, since convexity is not a measure invariant concept. In fact,

> *although the strain energy* $W^{J_2}(\epsilon_1, \epsilon_2, \epsilon_3)$*, Eq.* (8)*, is a strictly convex function for every deformation state, the strain energy* $\widehat{W}^{J_2}(\lambda_1, \lambda_2, \lambda_3)$ *is not always convex.*

In particular, using chain rule for composite functions, the Hessian of $\widehat{W}(\lambda_1, \lambda_2, \lambda_3)$ becomes

$$\frac{\partial^2 \widehat{W}}{\partial \lambda_i \partial \lambda_j} = \frac{1}{\lambda_i \lambda_j} \frac{\partial^2 W}{\partial \epsilon_i \partial \epsilon_j}, \quad i, j=1, 2, 3, \text{ (not summed)}, \tag{18}$$

so that an evaluation of its determinant for the J_2–deformation theory of plasticity and GBG material is sufficient to show that the strain energies $\widehat{W}(\lambda_1, \lambda_2, \lambda_3)$ are not always convex.

Strain softening (as well as convexity) is not a measure invariant concept, so that, to represent a 'material behaviour' it has to be understood in terms of true (Cauchy) stress components T_i as functions of the true (logarithmic) strain components ϵ_i. Therefore, to model strain softening, a nonconvexity of the strain energy $W(\epsilon_1, \epsilon_2, \epsilon_3)$ has been introduced in the GBG elasticity model.

Under plane strain condition (in the x_1–x_2 plane), the stress state for a GBG material, Eq. (10), generated by an uniaxial stress parallel to the x_1-direction is represented by the following principal Cauchy stress components,

$$T_1 = \frac{2}{\sqrt{3}} K \operatorname{sign}[\epsilon_1] \left[1 - \exp\left(-\frac{2|\epsilon_1|}{\sqrt{3}\epsilon_0}\right)\right] \times \exp\left(-\frac{2|\epsilon_1|}{\sqrt{3}c\epsilon_0}\right), \tag{19}$$

$$T_2 = 0, \quad T_3 = \frac{T_1}{2},$$

showing that the initial stiffness for plane strain uniaxial stress is $8K/3$. The uniaxial behaviour is shown for elongation logarithmic strain ($\epsilon_1 > 0$) versus Cauchy stress $(19)_1$ in the upper part of Fig. 2 and versus nominal stress, defined as

$$t_1 = T_1 \exp(-\epsilon_1), \tag{20}$$

in the lower part of Fig. 2, for the three different choices of parameters (A), (B) and (C) reported in Table 1.

Note from Fig. 2 that, in plane strain uniaxial stress, loss of positive definiteness of the fourth-order incremental constitutive tensor [see Eqs. (21) and (22)] occurs at the peak in the nominal stress curve (which corresponds to hardening in the true stress response), while loss of ellipticity occurs later (see Bigoni and Dal Corso 2008 for a detailed explanation of these concepts).

For special stress states, there can be simultaneity of loss of positive definiteness (Hill 1958 exclusion condition for bifurcation) and ellipticity (to be detailed later and corresponding to shear banding with discontinuity in the incremental strain field), so that in such a case there are no bifurcations prior to shear banding. Therefore, to investigate the effect of a Mode II perturbation

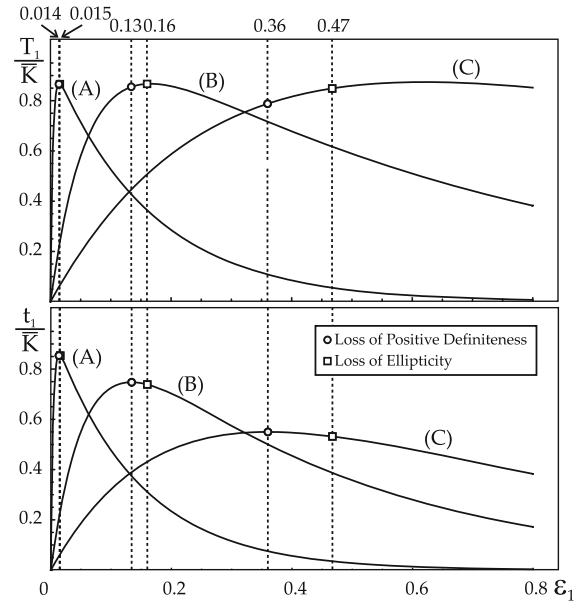

Fig. 2 Uniaxial plane strain tension response for GBG material [selected with constants defined in Table 1 as *(A)*, *(B)* and *(C)*]. Logarithmic strain ϵ_1 versus Cauchy stress T_1 (*upper part*) and nominal stress t_1 (*lower part*), normalized through division by $\overline{K} = 2{,}000$ MPa. Loss of positive definiteness of the fourth-order incremental constitutive tensor [see Eqs. (21) and (22)] and loss of ellipticity are marked with spots

Table 1 Sets of parameters for the GBG elastic model considered in the examples

GBG material parameters	c (−)	ϵ_0 (−)	K (MPa)
(A)	42	0.0045	1,680
(B)	10	0.0800	2,100
(C)	5	0.4000	2,600
(D)	600	0.1049	2,000
(E)	1,000	0.0195	2,000

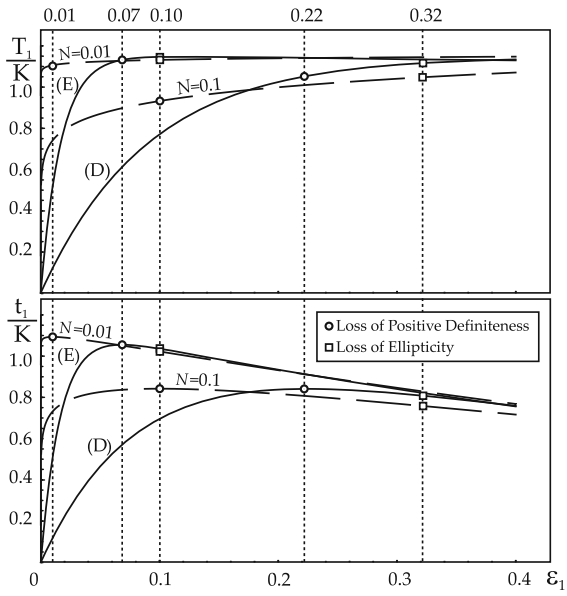

Fig. 3 Uniaxial plane strain tension response for GBG material [selected with constants defined in Table 1 as *(D)* and *(E)*] and J_2–deformation theory material (with $N = 0.01$ and 0.1). Logarithmic strain ϵ_1 versus Cauchy stress T_1 (*upper part*) and nominal stress t_1 (*lower part*), normalized through division by $K = 2{,}000$ MPa. Loss of positive definiteness of the elastic tensor and loss of ellipticity are marked with spots

on a slip surface aligned with a shear band that will be addressed later, we define loading processes for which the simultaneity is attained. The reason for this choice is that, after loss of positive definiteness and prior to shear banding, a slip surface becomes unstable in its straight configuration.

To compare the GBG material model with the J_2–deformation theory of plasticity is a difficult task, since these two models have been invented with different purposes. In particular, the former model has been tailored to represent quasi-brittle materials with softening, while the latter to describe ductile metals not evidencing softening in the true stress/true strain response. However, with the choice of hardening exponent $N = 0.01$ and 0.1 for the J_2–deformation theory material and with the choice of parameters (D) and (E) in Table 1 for the GBG material, we obtain a reasonable agreement between the two models, as shown in Fig. 3. The GBG material parameters listed as (D) and (E) are calibrated for the two models in such a way that loss of ellipticity occurs at the same value of logarithmic strain ϵ_1^E.

3 Incremental incompressible elasticity framework

The incremental behaviour described by the J_2–deformation theory of plasticity and GBG material falls within the constitutive framework for incompressible nonlinear elastic material given by Biot (1965, see also Bigoni and Dal Corso 2008). Within this framework, the material behaviour is decribed by the following linear relation between the increment of the nominal stress $\dot{\mathbf{t}}$ (transpose of the first Piola-Kirchhoff stress) and the transpose of the gradient of incremental displacement $\nabla\mathbf{v}$,

$$\dot{\mathbf{t}} = \mathbb{K}\left[\nabla\mathbf{v}^T\right] + \dot{p}\,\mathbf{I}, \tag{21}$$

where $(.)^T$ denotes the transpose, $\dot{p}$ represents the incremental in-plane mean stress and $\mathbb{K}$ is the fourth-order incremental constitutive tensor (possessing the major symmetry $\mathbb{K}_{ijhk} = \mathbb{K}_{hkij}$). Referring to the principal prestress axes system x_1–x_2, the only non-null components of the incremental constitutive tensor $\mathbb{K}$ are

$$\begin{aligned} &\mathbb{K}_{1111} = \mu(\xi - k - \eta), \quad \mathbb{K}_{2222} = \mu(\xi + k - \eta),\\ &\mathbb{K}_{2211} = \mathbb{K}_{1122} = -\mu\,\xi, \quad \mathbb{K}_{2121} = \mu(1 - k),\\ &\mathbb{K}_{1212} = \mu(1 + k), \qquad \mathbb{K}_{1221} = \mathbb{K}_{2112} = \mu(1 - \eta), \end{aligned} \tag{22}$$

where the following dimensionless quantities, depending on the prestress state (defined by the in-plane principal Cauchy stress components T_1 and T_2 and the two incremental moduli, μ for shear parallel and μ_* for shear inclined at $\pi/4$ with respect to the principal prestress axes x_1–x_2), are introduced

$$\xi = \frac{\mu_*}{\mu}, \quad \eta = \frac{T_1 + T_2}{2\mu}, \quad k = \frac{T_1 - T_2}{2\mu}. \tag{23}$$

For initially isotropic materials under plane strain condition, the deviatoric dimensionless parameter k becomes independent of the constitutive tensor and results to be given by Biot (1965)

$$k = \tanh(2\epsilon_1), \tag{24}$$

showing that $|k| < 1$. Note that $k = 0$ for null prestress, while $|k| \to 1$ when the strain tends to infinity.

The two incremental shear moduli μ and μ_* are functions of the strain energy $W(\lambda_1, \lambda_2, \lambda_3)$ in the form [see the Appendix A by Brun et al. (2003) for details],

$$\mu = \frac{1}{2}\frac{\lambda_1^2+\lambda_2^2}{\lambda_1^2-\lambda_2^2}\left(\lambda_1\frac{\partial \mathrm{W}}{\partial \lambda_1} - \lambda_2\frac{\partial \mathrm{W}}{\partial \lambda_2}\right),$$
$$\mu_* = \frac{1}{4}\left(\lambda_1\frac{\partial \mathrm{W}}{\partial \lambda_1} + \lambda_2\frac{\partial \mathrm{W}}{\partial \lambda_2} + \lambda_1^2\frac{\partial^2 \mathrm{W}}{\partial \lambda_1^2} + \lambda_2^2\frac{\partial^2 \mathrm{W}}{\partial \lambda_2^2} - 2\lambda_1\lambda_2\frac{\partial^2 \mathrm{W}}{\partial \lambda_1 \partial \lambda_2}\right), \tag{25}$$

which for a GBG material (7) become

$$\mu = \frac{K}{\sqrt{3}\,\tanh(2|\epsilon_1|)}\left[1-\exp\left(-\frac{2|\epsilon_1|}{\sqrt{3}\,\epsilon_0}\right)\right] \times \exp\left(-\frac{2|\epsilon_1|}{\sqrt{3}\,c\,\epsilon_0}\right),$$
$$\mu_* = \frac{K}{3\,c\,\epsilon_0}\left[(1+c)\exp\left(-\frac{2|\epsilon_1|}{\sqrt{3}\,\epsilon_0}\right)-1\right] \times \exp\left(-\frac{2|\epsilon_1|}{\sqrt{3}\,c\,\epsilon_0}\right), \tag{26}$$

so that, by the definition $(23)_1$, we find the ξ–ϵ_1 relationship

$$\xi = \frac{c\coth\left(\dfrac{\epsilon_1}{\sqrt{3}\epsilon_0}\right) - \mathrm{Sign}[\epsilon_1](2+c)}{2\sqrt{3}c\epsilon_0}\tanh(2\epsilon_1). \tag{27}$$

To treat incremental plane strain boundary value problems, it is instrumental to introduce a stream function

$$\psi(z) = \psi(x_1 + \Omega x_2), \tag{28}$$

related to the incremental displacements as follows,

$$v_1 = \frac{\partial \psi}{\partial x_2}, \quad v_2 = -\frac{\partial \psi}{\partial x_1}, \tag{29}$$

which automatically satisfies the incremental version of the incompressibility condition (5). The complex constant Ω appearing in Eq. (28) can be determined from the incremental equilibrium equations ($\dot{t}_{ij,i} = 0$) to take the four values

$$\Omega_j^2 = \frac{1-2\xi+(-1)^j\sqrt{4\xi^2-4\xi+k^2}}{1-k}, \quad j = 1,\ldots,4, \tag{30}$$

showing that the nature of the roots Ω_j changes as a function of parameters ξ and k. We define

$$\Omega_j = \alpha_j + i\beta_j, \tag{31}$$

where $i = \sqrt{-1}$ is the imaginary unit and $\alpha_j = \mathfrak{Re}\,[\Omega_j]$ and $\beta_j = \mathfrak{Im}\,[\Omega_j]$ ($\mathfrak{Re}\,[\cdot]$ and $\mathfrak{Im}\,[\cdot]$ denote the real and imaginary part of the relevant argument).

In the following we restrict our attention to the Elliptic regime (E), corresponding to the absence of real roots, namely,

$$\beta_j \neq 0, \quad j = 1,\ldots,4, \tag{32}$$

representing deformation states for which shear bands (in terms of discontinuities in incremental strain field) are excluded.[4] In particular, the elliptic regime can be subdivided into elliptic imaginary (EI) and elliptic complex (EC) regimes. The elliptic imaginary regime (EI) is defined by the conditions

$$k^2 < 1 \quad \text{and} \quad 2\xi > 1+\sqrt{1-k^2}, \tag{33}$$

corresponding to four imaginary conjugate roots Ω_j, so that

$$\alpha_1 = \alpha_2 = 0,$$
$$\left.\begin{matrix}\beta_1\\ \beta_2\end{matrix}\right\} = \sqrt{\frac{2\xi-1\pm\sqrt{4\xi^2-4\xi+k^2}}{1-k}} > 0, \tag{34}$$

while the elliptic complex (EC) regime is defined by the conditions

$$k^2 < 1 \quad \text{and} \quad 1-\sqrt{1-k^2} < 2\xi < 1+\sqrt{1-k^2}, \tag{35}$$

corresponding to four complex conjugate roots Ω_j, so that

$$\left.\begin{matrix}\beta = \beta_1 = \beta_2\\ \alpha = -\alpha_1 = \alpha_2\end{matrix}\right\} = \sqrt{\frac{\sqrt{1-k^2}\pm(2\xi-1)}{2(1-k)}} > 0. \tag{36}$$

For GBG material, we note from Eqs. (26)–(27) that for null prestrain ($\epsilon_1 = 0$) we obtain

$$\mu(\epsilon_1=0) = \mu_*(\epsilon_1=0) = \frac{K}{3\epsilon_0}, \quad \xi(\epsilon_1=0) = 1, \tag{37}$$

showing that the initial material behaviour is isotropic, while in the limit of infinite prestrain ($\epsilon_1 \to \infty$),

$$\xi = -\frac{1}{\sqrt{3}c\epsilon_0} < 0, \tag{38}$$

so that at 'large enough strain' for GBG material μ_* becomes negative, an effect that is related to softening and does not occur for the J_2–deformation theory material, where $\xi \geq 0$ for every ϵ_1.

[4] Parabolic (P) and Hyperbolic (H) regimes are attained when the roots Ω_j assume two and four real values, respectively.

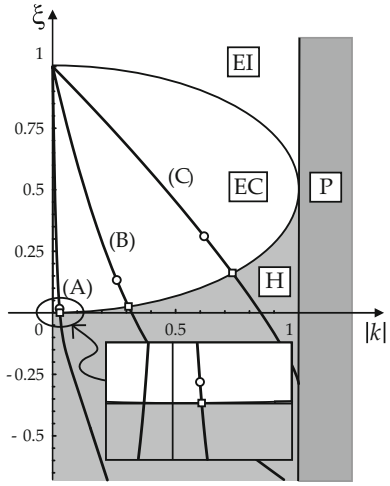

Fig. 4 Deformation paths in the ξ–k plane for the GBG materials with the parameter combinations *(A)*, *(B)* and *(C)* reported in Table 1. Note that ξ becomes negative at sufficiently high prestress k

Combination of Eqs. (27) and (24) yields

$$\xi = \frac{1}{2\sqrt{3}\epsilon_0}\left[\frac{\left(\frac{1+k}{1-k}\right)^{\frac{1}{2\sqrt{3}\epsilon_0}}+1}{\left(\frac{1+k}{1-k}\right)^{\frac{1}{2\sqrt{3}\epsilon_0}}-1}k - \frac{2+c}{c}|k|\right], \quad (39)$$

describing all possible deformation paths for the GBG material by a curve in the ξ–k plane, depending on the values of the material constitutive parameters (c, ϵ_0).[5] Typical deformation paths are reported in Fig. 4 for GBG material with the parameter combinations (A), (B) and (C) reported in Table 1. In Fig. 5 both the behaviours of the J_2–deformation theory and GBG materials are reported, where the selected parameters are $N = 0.01$ and 0.1 for the former material model and (D) and (E) listed in Table 1 for the latter.

With reference to the deformation paths shown in Figs. 4 and 5, the values of logarithmic deformation ϵ_1 for which loss of positive definiteness (in uniaxial plane strain, $\varepsilon_1^{\mathrm{PD}}$) and loss of ellipticity (ε_1^{E}) occur for the incremental constitutive tensor $\mathbb{K}$, Eq. (22), are reported in Table 2 (together with the predicted inclination of the shear band, ϑ^{SB}, measured from the principal prestress axis x_1).

[5] From relation (39), it follows that the ratio of incremental shear stiffness depends only on the absolute value of k, in other words, $\xi(k) = \xi(-k)$.

From the deformation paths shown in Fig. 5 we may conclude:

- while the J_2–deformation theory material is initially (for $k = 0$) orthotropic and singular (the initial tangent stiffness is infinite), the GBG material is initially isotropic $\xi = 1$ and nonsingular (the initial tangent stiffness is $8K/3$);
- the way in which the GBG material traverses the $\xi - k$ plane to approach the boundary of ellipticity is much 'steeper' than for the J_2–deformation theory material. This means that the incremental response of the GBG material becomes anisotropic (parameter ξ) much faster with continuing deformation than the response of the J_2–deformation theory material.

4 Slip surface and rigid line inclusion

Since slip surfaces and rigid line inclusions can be in general inclined with respect to the Lagrangean axes defining the state of prestress, it becomes instrumental now to introduce a rotated reference system where to express the incremental constitutive Eq. (21).

Considering a $\hat{x}_1$–$\hat{x}_2$ reference system rotated at an angle ϑ_0 with respect to the principal prestress axes x_1–x_2,

$$\hat{\mathbf{x}} = \mathbf{Q}^T\mathbf{x}, \quad [\mathbf{Q}] = \begin{bmatrix} \cos\vartheta_0 & \sin\vartheta_0 \\ -\sin\vartheta_0 & \cos\vartheta_0 \end{bmatrix}, \quad (40)$$

the incremental linear constitutive relation (21) can be rewritten in the inclined system as

$$\hat{\mathbf{t}} = \widehat{\mathbb{K}}[\hat{\nabla}\hat{\mathbf{v}}^T] + \dot{p}\,\mathbf{I}, \quad (41)$$

where the nominal stress increment ($\hat{\mathbf{t}}$), incremental displacement gradient ($\hat{\nabla}\hat{\mathbf{v}}$), and the constitutive tensor ($\widehat{\mathbb{K}}$) in the $\hat{x}_1$–$\hat{x}_2$ reference system are respectively given by

$$\hat{\mathbf{t}} = \mathbf{Q}^T\mathbf{t}\mathbf{Q}, \quad \hat{\nabla}\hat{\mathbf{v}} = \mathbf{Q}^T\nabla\mathbf{v}\mathbf{Q},$$
$$\widehat{\mathbb{K}}_{ijhk} = Q_{li}Q_{mj}\mathbb{K}_{lmno}Q_{nh}Q_{ok}. \quad (42)$$

Therefore, we can introduce a stream function $\widehat{\psi}(\hat{z})$ where

$$\hat{z}_j = \hat{x}_1 + W_j\,\hat{x}_2, \quad W_j = \frac{\sin\vartheta_0 + \Omega_j\cos\vartheta_0}{\cos\vartheta_0 - \Omega_j\sin\vartheta_0}, \quad (43)$$
$$j = 1, \ldots, 4,$$

and the relation (29) can be now defined in the $\hat{x}_1 - \hat{x}_2$ reference system as

$$\hat{v}_1 = \frac{\partial\widehat{\psi}}{\partial\hat{x}_2}, \quad \hat{v}_2 = -\frac{\partial\widehat{\psi}}{\partial\hat{x}_1}. \quad (44)$$

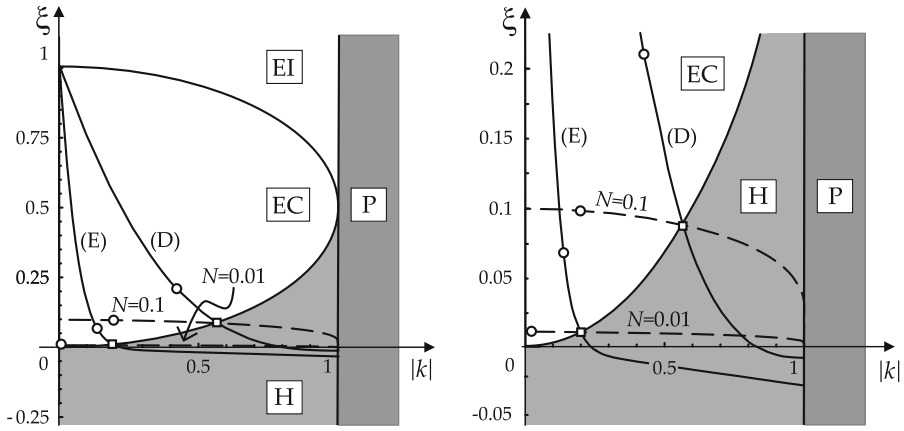

Fig. 5 Stress paths in the ξ–k plane for GBG material [with the parameter combinations *(D)* and *(E)* reported in Table 1] and J_2–deformation theory of plasticity ($N = 0.1$ and $N = 0.01$). Note that the anisotropization rate is higher in the latter material than in the former, so that the GBG material 'runs faster' to loss of ellipticity than the deformation theory of plasticity. The right part of the figure is a detail of the left one

Table 2 Critical logarithmic strains corresponding to loss of positive definiteness (in uniaxial plane strain, $\varepsilon_1^{\mathrm{PD}}$) and ellipticity ($\varepsilon_1^{E}$) of the incremental elastic tensor $\mathbb{K}$, Eq. (22), for GBG elastic material subject to uniaxial tension (positive sign) and compression (negative sign) parallel to the x_1–axis, for the parameter sets reported in Table 1

Material parameters	PD ϵ_1^{PD}	E ε_1^{E}	Uniaxial tension ϑ^{SB} (°)	Uniaxial compression ϑ^{SB} (°)
(A)	±0.014	±0.015	±44.580	±45.420
(B)	±0.134	±0.160	±40.447	±49.553
(C)	±0.360	±0.467	±32.084	±57.916
(D)	±0.224	±0.322	±35.942	±54.058
(E)	±0.068	±0.100	±42.135	±47.865

Full-field, closed-form solutions for incremental deformation/stress applied at infinity can be obtained for homogeneously prestressed materials[6] containing a line inclusion (of length 2l) aligned parallel to the $\hat{x}_1$–axis ($|\hat{x}_1| < l$, $\hat{x}_2 = 0$) and inclined at an angle[7] ϑ_0 with respect to the principal prestress axes x_1–x_2. The presence of the inclusion introduces further boundary conditions on the incremental mechanical fields along the line where the inclusion lies. In particular, we consider the following two models of inclusion.

- Slip surface, imposing null incremental nominal shearing tractions, continuity of the incremental nominal normal traction and of normal incremental displacement on the slip line, namely

$$\begin{cases} \hat{t}_{21}(\hat{x}_1, 0^{\pm}) = 0, \\ [\![\hat{t}_{22}(\hat{x}_1, 0)]\!] = 0, \quad \forall |\hat{x}_1| < l, \\ [\![\hat{v}_2(\hat{x}_1, 0)]\!] = 0, \end{cases} \tag{45}$$

  where the brackets $[\![\cdot]\!]$ denotes the jump in the relevant argument, taken across the inclusion.
- Rigid line inclusion, imposing incremental kinematical boundary conditions on the stiffener line (which may only suffer a rigid-body motion) and integral statical boundary condition for the incremental 'global' equilibrium of the inclusion. Considering material and loading symmetries and the particular form of the solution that will be found, Eq. (47)$_1$, the incremental boundary conditions for

[6] The presence of an inclusion within a material introduces a stress concentration and therefore the deformation and stress states result to be in general highly inhomogeneous. Nevertheless, we can reach at imposed finite deformation an homogeneous prestress when the inclusion is neutral to the deformation process, corresponding to a uniform Mode I for a slip surface and uniform simple shear for a rigid line inclusion. At a certain stage of this deformation process, a perturbation can be introduced by an incremental Mode II and Mode I, respectively.

[7] The inclination of the inclusion with respect to the principal prestress axes, ϑ_0, is taken to be equal to

Footnote 7 continued

- the predicted inclination of the shear band at the elliptic boundary, ϑ^{SB}, for the slip surface problem;
- the inclination between the principal axes and the inclusion line, during a simple shear parallel to the inclusion, $\vartheta^{E} = \frac{1}{2}\arctan\left(2\lambda_1/(\lambda_1^2 - 1)\right)$, for the stiffener problem.

the stiffener problem can be reduced to the following independent boundary conditions:

$$\begin{cases} \hat{v}_{1,1}(\hat{x}_1, 0) = 0, \\ [\![\hat{v}_{2,1}(\hat{x}_1, 0)]\!] = 0, \quad \forall\, |\hat{x}_1| < l, \\ [\![\hat{t}_{22}(\hat{x}_1, 0)]\!] = 0. \end{cases} \tag{46}$$

In both cases of slip surface and rigid line inclusion, the solution can be obtained using the linear superposition principle and summing the solutions of two different problems where an homogeneously prestressed infinite material (without inclusion) is considered. The first problem, corresponding to imposed stress/strain at infinity, has the trivial solution of a homogenous state ($\widehat{\psi}^{\infty}$), while in the second we consider the infinite material subject to boundary conditions on deformation/traction along the line where the inclusion lies, such that the boundary conditions (45) or (46) on the inclusion interface are recovered for the total problem. The solution of the latter problem is represented by the stream function $\widehat{\psi}^{\circ}$, which is in the form

$$\hat{\psi}^{\circ}(\hat{x}_1, \hat{x}_2) = \hat{a} \sum_{j=1}^{2} \mathfrak{Re}\left[A_j f(\hat{z}_j)\right], \tag{47}$$

where

$$f(\hat{z}_j) = \hat{z}_j^{\,2} - \hat{z}_j \sqrt{\hat{z}_j^{\,2} - l^2} + l^2 \ln\left(\hat{z}_j + \sqrt{\hat{z}_j^{\,2} - l^2}\right), \tag{48}$$

and

$$\hat{a} = \begin{cases} \dfrac{\hat{t}_{21}^{\infty}}{2\mu}, & \text{slip surface}, \\ \dfrac{\hat{v}_{2,2}^{\infty}}{2}, & \text{stiffener}. \end{cases} \tag{49}$$

Incremental boundary conditions for the slip surface (45) and for the stiffener (46) lead to two different systems of four linear equations in the unknown complex constants $A_j (j = 1, 2)$. Two of these linear equations are common to both problems,

slip surface/stiffener

$$\begin{cases} \mathfrak{Im}[A_1] + \mathfrak{Im}[A_2] = 0, \\ -c_{21}\mathfrak{Re}[A_1] + c_{11}\mathfrak{Im}[A_1] \\ \quad -c_{22}\mathfrak{Re}[A_2] + c_{12}\mathfrak{Im}[A_2] = 0, \end{cases} \tag{50}$$

while the other two differs for the slip surface,

slip surface

$$\begin{cases} c_{31}\mathfrak{Re}[A_1] + c_{41}\mathfrak{Im}[A_1] + c_{32}\mathfrak{Re}[A_2] \\ \quad +c_{42}\mathfrak{Im}[A_2] = -1, \\ -c_{41}\mathfrak{Re}[A_1] + c_{31}\mathfrak{Im}[A_1] \\ \quad -c_{42}\mathfrak{Re}[A_2] + c_{32}\mathfrak{Im}[A_2] = 0, \end{cases} \tag{51}$$

and for the rigid line inclusion,

stiffener

$$\begin{cases} \mathfrak{Re}[W_1]\mathfrak{Re}[A_1] - \mathfrak{Im}[W_1]\mathfrak{Im}[A_1] \\ \quad +\mathfrak{Re}[W_2]\mathfrak{Re}[A_2] - \mathfrak{Im}[W_2]\mathfrak{Im}[A_2] = 1, \\ \mathfrak{Im}[W_1]\mathfrak{Re}[A_1] + \mathfrak{Re}[W_1]\mathfrak{Im}[A_1] \\ \quad +\mathfrak{Im}[W_2]\mathfrak{Re}[A_2] + \mathfrak{Re}[W_2]\mathfrak{Im}[A_2] = 0, \end{cases} \tag{52}$$

where the real coefficients c_{ij} (functions of the prestress state and of the inclination of the inclusion with respect to the principal stress axes ϑ_0) are given in Appendix A by Eqs. (A 1).

The modulus of incremental deviatoric strain obtained from the perturbed solutions $\widehat{\psi}^{\circ}$ are plotted for a slip surface (Fig. 6) and a stiffener (Fig. 7) in a material prestrained (and thus prestressed) through a deformation $\epsilon_1 = -\epsilon_2$, at different distances from the elliptic boundary (corresponding to ϵ_1^E).

The slip surface (stiffener) is strained through a horizontal tensile strain ϵ_1 (a simple shear, with principal strain ϵ_1) and perturbed by an incremental Mode II (Mode I) loading, uniform at infinity. In both Figs. 6 and 7, the responses are reported for the GBG material, with the set (D) of parameters (Table 1), and for the J_2–deformation theory material at low hardening, $N = 0.1$.

The slip surface is taken parallel to one of the shear band directions which correspond to ellipticity loss (inclinations are provided in Table 2 for GBG material, while for the J_2–material, the inclination can be calculated from Bigoni and Dal Corso (2008), their Eqn. A16). Moreover, the ratio η/k is chosen in a way that the positive definiteness of tensor $\mathbb{K}$ (so-called 'Hill 1958 exclusion condition') and ellipticity are lost simultaneously.

Since for the stiffener problem the simple shear is aligned with the stiffener, one of the shear band inclinations at ellipticity loss results also to be almost[8] aligned with the stiffener (in the horizontal direction in Fig. 7).

We may observe from Fig. 6 that the strain increment results to be strongly focussed parallel to the direction of the slip surface (while the other shear band direction results to be completely inactive), indicating that this

[8] In our framework it is possible to choose the stiffener at every inclination with respect to the current state of prestress. However, we prefer to generate the state of prestress by imposing a finite simple shear parallel to the inclusion itself. In this way, the stiffener is neutral, but it results only 'almost aligned' with one of the shear bands. However, the discrepancy in the inclination is so small that does not appreciably alter results.

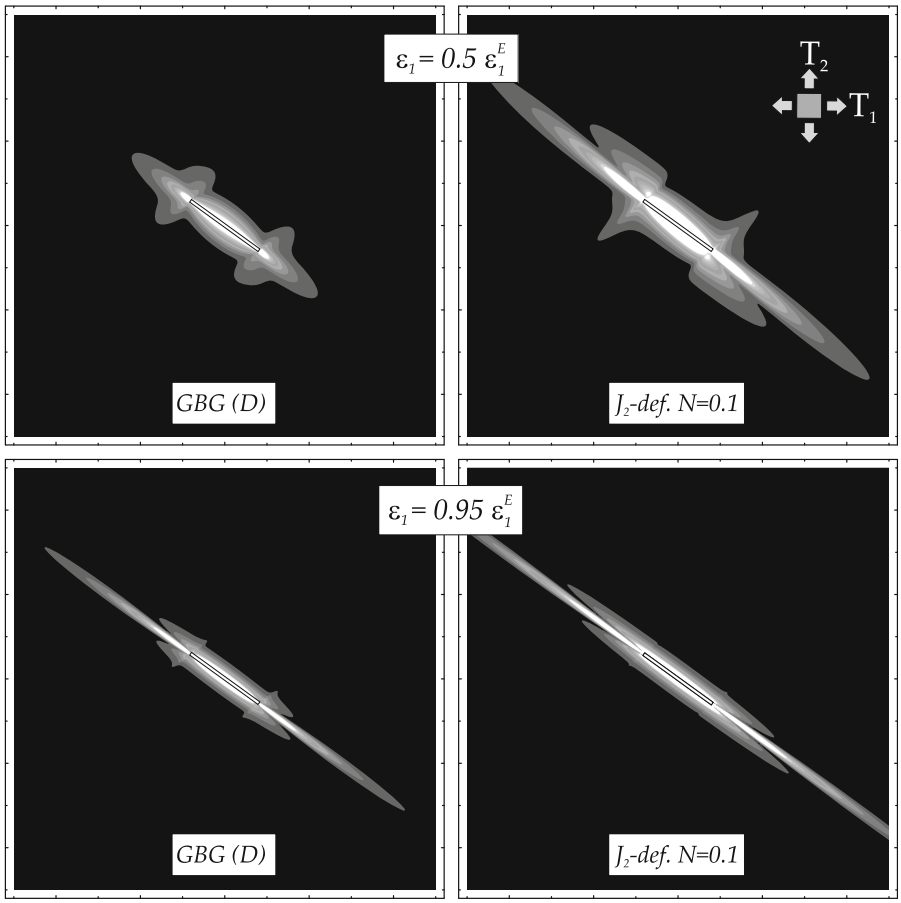

Fig. 6 A slip surface embedded in J_2 and GBG elastic materials at different level of prestrain ϵ_1 (corresponding to a uniform stress state) is perturbed through a Mode II loading, uniform at infinity. The level sets of the modulus of the incremental deviatoric strain are reported. The parameter η/k has been selected such that positive definiteness of the constitutive tensor $\mathbb{K}$, Eq. (22), is satisfied

is a privileged mode of failure. On the other hand, the stiffener, Fig. 7, represents an obstacle to shear band propagation, so that the incremental deformation fields show that the band inclined with respect to the stiffener is almost completely inhibited, while that aligned 'nearly parallel' develops less than in the case of the slip surface.

At a prestrain $\epsilon_1 = 0.5\epsilon_1^E$ the perturbation produced by the slip surface evidences strain localization for the J_2–deformation theory material (already near the elliptic boundary), but not for the GBG material (still far from the elliptic boundary). This conclusion is valid both for the slip surface and for the stiffener, although it is more evident in the former than in the latter case. This effect is substantiated by the fact that the GBG material has an anisotropization rate much higher than the J_2–deformation theory material, implying that the boundary of ellipticity is approached nearly orthogonal in the ξ–k plane, see Figs. 4 and 5. As a consequence, the sensibility to perturbations is different in the two materials.

The growth of an inclusion (slip surface and stiffener in our case) can be analysed considering the incremental energy release rate associated to an infinitesimal inclusion advance. This quantity results to be written as (see Bigoni and Dal Corso et al. (2008); Dal Corso and Bigoni (2009) for details)

$$\dot{G}_{II} = \dot{K}_{II}^2 \frac{\mathfrak{Im}\,[W_1 A_1 + W_2 A_2]}{4\mu}, \tag{53}$$

for an advance of the slip surface under Mode II and

$$\dot{G}_I = -\frac{\dot{K}_{(\epsilon)\,I}^2}{8\mu^2}\Big\{\big[\widehat{\mathbb{K}}_{2121} - 2(\mathfrak{Re}\,[A_1] + \mathfrak{Re}\,[A_2])(\widehat{\mathbb{K}}_{2221} - \widehat{\mathbb{K}}_{2111})\big]\,\mathfrak{Im}\,[W_1^2 A_1 + W_2^2 A_2] + 2(\mathfrak{Re}\,[A_1] + \mathfrak{Re}\,[A_2])\widehat{\mathbb{K}}_{2121}\,\mathfrak{Im}\,[W_1^3 A_1 + W_2^3 A_2]\Big\}. \tag{54}$$

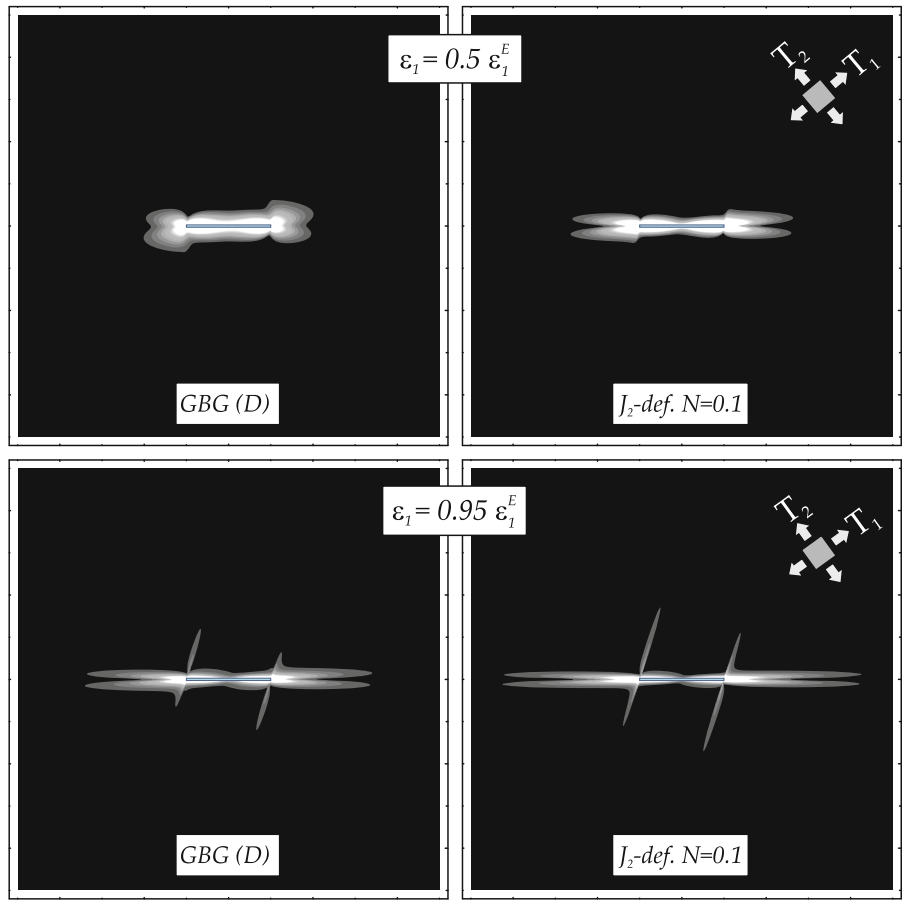

Fig. 7 A rigid line inclusion embedded in J_2 and GBG elastic materials at different level of prestrain ϵ_1 (generated by a simple shear parallel to the inclusion line) is perturbed through a Mode I loading, uniform at infinity ($\eta/k = 1$ has been used). The level sets of the modulus of the incremental deviatoric strain are reported

for an advance of the rigid line inclusion under Mode I, where

$$\begin{cases} \dot{K}_I = \lim_{\hat{x}_1 \to l^+} \sqrt{2\pi\,(\hat{x}_1 - l)} \\ \qquad \times \hat{t}_{21}(\hat{x}_1, \hat{x}_2 = 0), \text{ slip surface}, \\ \dot{K}_{(\epsilon)\,I} = 2\mu \lim_{\hat{x}_1 \to l^+} \sqrt{2\pi\,(\hat{x}_1 - l)} \\ \qquad \times \hat{v}_{2,2}(\hat{x}_1, \hat{x}_2 = 0), \text{ stiffener}, \end{cases} \tag{55}$$

representing incremental stress intensity factors, which for uniform incremental loading at infinity correspond to

$$\begin{cases} \dot{K}_I = \hat{t}_{21}^{\infty} \sqrt{\pi l}, & \text{slip surface}, \\ \dot{K}_{(\epsilon)\,I} = 2\mu\, \hat{v}_{2,2}^{\infty} \sqrt{\pi l}, & \text{stiffener}. \end{cases} \tag{56}$$

Note that $\dot{G}_I(\dot{G}_{II})$ always results positive (negative), meaning that the slip surface (stiffener) tends to increase (reduce) its length. The essential point here is that for a slip surface (stiffener) loaded under Mode II (Mode I) the incremental energy release rate blows up to infinite (decays to zero) when the elliptic boundary is approached, so that the growth of the slip surface (reduction of the stiffener) results strongly promoted (inhibited). These features are shown in Figs. 8 and 9, where the incremental energy release rate $\dot{G}_{II}$ and $\dot{G}_I$ are plotted respectively as functions of the prestrain parameter ϵ_1. This result means that while a slip surface aligned with a shear band tends to become a dominant failure mechanism near the elliptic border, a rigid line inclusion tends to represent a 'modest' obstacle to shear band growth along its direction.[9]

[9] In the Figs. 8 and 9 a different normalization of the incremental energy release rate from those employed by Bigoni and Dal Corso (2008) and Dal Corso and Bigoni (2009) has been used [so that for instance, the incremental energy release rate vanishes at null prestrain for J_2–material, while this was not the case for the graphs reported by Bigoni and Dal Corso (2008)].

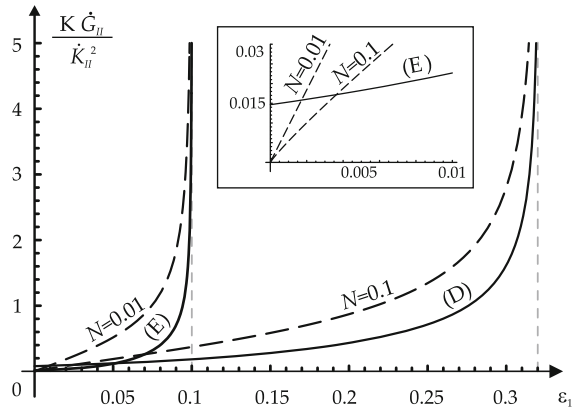

Fig. 8 Mode II incremental energy release rate for slip surface growth in prestrained J_2 [$N = 0.01$ and $N = 0.1$] and GBG [cases (E) and (D), Table 1] materials (prestrain parameter is ϵ_1). The slip surface is aligned parallel with a shear band direction. Note the difference between the two models in the rate of blow up, when the ellipticity limit ($\epsilon_1 = \{0.1; 0.322\}$) is approached. A detail of the behaviour near the origin is shown in the inselt

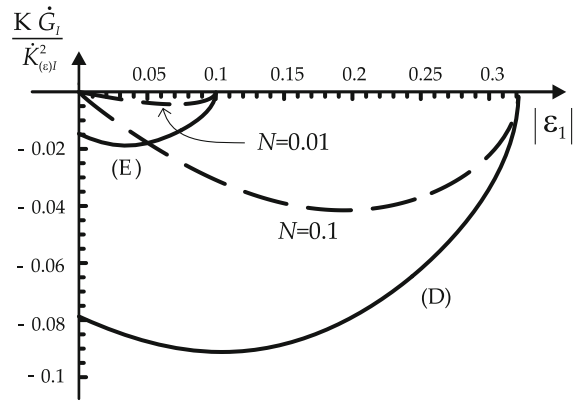

Fig. 9 Mode I incremental energy release rate for rigid line inclusion reduction (negative growth) in prestrained J_2 [$N = 0.01$ and $N = 0.1$] and GBG [cases (E) and (D), Table 1] materials (prestrain parameter is ϵ_1). The rigid line inclusion is aligned parallel with a shear band direction. Note the difference between the two models in the rate of decay to zero, when the ellipticity limit ($\epsilon_1 = \{0.1; 0.322\}$) is approached

A conclusion that can be drawn from Figs. 8 and 9 is that the stronger anisotropization rate with prestrain of the GBG material, compared to the J_2–material, implies that the blow up (decay) of the curves for the slip surface (stiffener) when the elliptic border is approached is much steeper for GBG material than for the J_2–material. Therefore, we can point out that the GBG material 'runs faster to instability' than the J_2–deformation theory material, a feature connected to the softening effect inherent to the GBG material model.

5 Conclusions

Slip surfaces aligned parallel to a shear band direction (which may model both a pre-existing shear band or a fracture aligned with a shear band) in a prestressed material near the elliptic boundary have been shown to be preferential failure modes (propagating rectilinearly under Mode II loading) for a material model exhibiting strain softening at large strain in the true-stress/true-strain response. This conclusion follows from the achievement of a closed-form solution (under uniform Mode II loading) showing: (i.) a strong focussing of the incremental deformation produced by the slip surface and (ii.) a blowing up of the incremental energy release rate for surface growth. Evaluation of the same quantities (but under Mode I loading) when an obstacle to the propagation (modelled as a rigid line inclusion) is present along a shear band direction, suggests that the obstacle does not offer a sensible contrast to shear band growth.

Acknowledgments The authors thank Professors F.D. Fischer and W. Daves (University of Leoben) for helpful discussions. Financial support from PRIN grant n. 2007YZ3B24 'Multi-scale Problems with Complex Interactions in Structural Engineering' from the Italian Ministry of University and Research is also gratefully acknowledged.

Appendix A. Values of coefficients c_{ij}

The real coefficients c_{ij}, appearing in the linear Eqs. (50)–(51), depending on the inclusion inclination ϑ_0, prestress and orthotropy parameters ξ, k and η, are

$$
\begin{aligned}
2\,\mu\, c_{1j} &= \widehat{\mathbb{K}}_{1112} - \widehat{\mathbb{K}}_{1222} - \mathfrak{Re}\,[W_j]\left[\widehat{\mathbb{K}}_{1111}\right.\\
&\quad -2\widehat{\mathbb{K}}_{1122} - \widehat{\mathbb{K}}_{1221} + \widehat{\mathbb{K}}_{2222} + \mathfrak{Re}\,[W_j]\\
&\quad \times \left(2\widehat{\mathbb{K}}_{1121} - 2\widehat{\mathbb{K}}_{2122} + \mathfrak{Re}\,[W_j]\widehat{\mathbb{K}}_{2121}\right)\Big]\\
&\quad +\mathfrak{Im}\,[W_j]^2\left(2\widehat{\mathbb{K}}_{1121} - 2\widehat{\mathbb{K}}_{2122}\right.\\
&\quad \left.+3\mathfrak{Re}\,[W_j]\widehat{\mathbb{K}}_{2121}\right),\\
2\,\mu\, c_{2j} &= \mathfrak{Im}\,[W_j]\left[\widehat{\mathbb{K}}_{1111} - 2\widehat{\mathbb{K}}_{1122} - \widehat{\mathbb{K}}_{1221} + \widehat{\mathbb{K}}_{2222}\right.\\
&\quad +\mathfrak{Re}\,[W_j]\left(4\widehat{\mathbb{K}}_{1121} - 4\widehat{\mathbb{K}}_{2122}\right.\\
&\quad \left.\left.+3\mathfrak{Re}\,[W_j]\widehat{\mathbb{K}}_{2121}\right) - \mathfrak{Im}\,[W_j]^2\widehat{\mathbb{K}}_{2121}\right],\\
2\,\mu\, c_{3j} &= -\widehat{\mathbb{K}}_{1221} + \mathfrak{Re}\,[W_j]\\
&\quad \times \left[\widehat{\mathbb{K}}_{1121} - \widehat{\mathbb{K}}_{2122} + \mathfrak{Re}\,[W_j]\widehat{\mathbb{K}}_{2121}\right)\\
&\quad -\mathfrak{Im}\,[W_j]^2\widehat{\mathbb{K}}_{2121},\\
2\,\mu\, c_{4j} &= \mathfrak{Im}\,[W_j]\left(-\widehat{\mathbb{K}}_{1121} + \widehat{\mathbb{K}}_{2122}\right.\\
&\quad \left.-2\mathfrak{Re}\,[W_j]\widehat{\mathbb{K}}_{2121}\right),\ j = 1, 2.
\end{aligned}
\tag{A 1}
$$

References

Bigoni D, Dal Corso F (2008) The unrestrainable growth of a shear band in a prestressed material. Proc R Soc A 464:2365–2390

Bigoni D, Dal Corso F, Gei M (2008) The stress concentration near a rigid line inclusion in a prestressed, elastic material. Part II implications on shear band nucleation, growth and energy release rate. J Mech Phys Solids 56:839–857

Biot MA (1965) Mechanics of incremental deformations. Wiley, New York

Brun M, Capuani D, Bigoni D (2003) A boundary element technique for incremental, non-linear elasticity. Part I: formulation. Comput Methods Appl Mech Eng 192:2461–2479

Dal Corso F, Bigoni D (2009) The interactions between shear bands and rigid lamellar inclusions in a ductile metal matrix. Proc R Soc A 465:143–163

Dal Corso F, Bigoni D, Gei M (2008) The stress concentration near a rigid line inclusion in a prestressed, elastic material. Part I full-field solution and asymptotics. J Mech Phys Solids 56:815–838

Gei M, Bigoni D, Guicciardi S (2004) Failure of silicon nitride under uniaxial compression at high temperature. Mech Mater 36:335–345

Hill R (1958) A general theory of uniqueness and stability in elastic-plastic solids. J Mech Phys Solids 6:236–249

Neale KW (1981) Phenomenological constitutive laws in finite plasticity. SM Arch 6:79–128

Ogden RW (1984) Non-linear elastic deformations. Ellis Horwood, Chichester

Trapper P, Volokh KY (2008) Cracks in rubber. Int J Solids Struct 45:6034–6044

Volokh KY (2007) Hyperelasticity with softening for modeling materials failure. J Mech Phys Solids 55:2237–2264